

New Interpretation for Laser Light Scattering Technique

Yong Sun*

November 19, 2018

Abstract

The new method proposed in this work not only measures the particle size distribution and the average molar mass accurately using the static light scattering (SLS) technique when the Rayleigh-Gans-Debye approximation is valid for dilute poly-disperse homogenous spherical particles in dispersion, but also enables us to have insight into the theoretical analysis of the dimensionless shape parameter ρ . With the method, a new size, static radii R_s , can be measured. Based on the new static particle size information, detailed investigation of the normalized time auto-correlation function of the scattered light intensity $g^{(2)}(\tau)$ reveals that there exist three different particle sizes: the static radius, hydrodynamic radius and apparent hydrodynamic radius that is the hydrodynamic radius obtained using the cumulants method. With a simple assumption that the hydrodynamic radius R_h is in proportion to the static radius R_s , the expected values of $g^{(2)}(\tau)$ calculated based on the static and commercial particle size information are consistent with the experimental data. With the assistance of simulated data, the apparent hydrodynamic radius is discussed. The results show that the apparent hydrodynamic radius is different from the mean hydrodynamic radius and is determined by the optical, hydrodynamic characteristics and size distribution of particles and scattering vector. The analysis also reveals that ρ is determined by not only the structure of particles but also the relationship between the optical and hydrodynamic characteristics of particles even for mono-disperse model.

1 INTRODUCTION

For colloidal dispersion systems, light scattering is a widely used technique to measure the sizes of particles. In dynamic light scattering (DLS) technique, the standard method of cumulants [1–4] has been used to measure the hydrodynamic radius, or more strictly apparent hydrodynamic radius $R_{h,app}$ [5] of particles from the normalized time auto-correlation function of the scattered light intensity $g^{(2)}(\tau)$ with the assistance of the Einstein-Stokes relation, where

*Email: ysun2002h@yahoo.com.cn

τ is the delay time. $g^{(2)}(\tau)$ is considered to be determined by the hydrodynamic radius and the scattering vector q for dilute homogenous spherical particles [2]. The treatment of the static light scattering (SLS) data is simplified to the Zimm plot, Berry plot or Guinier plot etc. to get the root mean-square radius of gyration $\langle R_g^2 \rangle^{1/2}$ and the molar mass of particles provided that the particle sizes are small [4, 6]. For a long time, the measurements of the dimensionless shape parameter $\rho = \langle R_g^2 \rangle^{1/2} / R_{h,app}$ [6–10] have been extensively used to infer the structures of particles. In this judgement, it has an assumption that the particle sizes measured from SLS and DLS are the same.

For large particles, DLS technique, where it loses the accuracy of size measurements, is endeavored to use at different scattering vectors in order to obtain the effective diffusion coefficient [11] or the apparent hydrodynamic radius [5] to detect small poly-dispersities. The standard DLS techniques are not suited to the accurate determination for the poly-dispersities (standard deviation/mean size) less than about 10%. For dilute poly-disperse homogeneous spherical particles, Pusey and van Meegen [11] proposed a method to detect small poly-dispersities when the Rayleigh-Gans-Debye (RGD) approximation is valid for the particles with the mean radius larger than 170 nm. In their treatment, the effective diffusion coefficient is obtained from the initial slope of the logarithm of the correlation function with respect to the scattering vector. By their definition, the effective diffusion coefficient is an intensity-weighted average diffusion coefficient. Both their theoretical and experimental results show that the angular dependence of the effective diffusion coefficient is a sensitive function of the particle size and distribution.

SLS technique has been reported to measure the particle size distribution by some groups. Strawbridge and Hallett [12] studied the theoretical scattered intensity of coated spheres with vertically polarized incident light. The scattered intensity at the geometrical or linear trial radii between r_{\min} and r_{\max} was used to fit the SLS data. Schnablegger and Glatter [13] assumed that the particle size distribution can be described as a series of cubic B-splines and used the simulated and measured data to demonstrate the computation procedure.

In this work, a SLS treatment is reported for the size information of the dilute poly-disperse homogeneous spherical particles in dispersion. The number distribution of particle sizes is assumed to be Gaussian and the effects of the scattering vector and the different intensity weights of different particle sizes on the scattered light intensity are considered. With the assistance of a non-linear least squares fitting program, the mean static radius $\langle R_s \rangle$ and the standard deviation σ are measured accurately. Given the absolute magnitude of the scattered intensity and some parameters related to the instrument and samples, the average molar mass can also be measured accurately. Based on the static particle size information, detailed investigation of the normalized time auto-correlation function of the scattered light intensity $g^{(2)}(\tau)$ reveals that there exist three different particle sizes: a static radius is measured from the optical characteristics, a hydrodynamic radius is obtained from the hydrodynamic features and an apparent hydrodynamic radius that is the hydrodynamic radius obtained using

the cumulants method is determined by the optical and hydrodynamic characteristics of particles. With a simple assumption that the hydrodynamic radius R_h is in proportion to the static radius R_s , the expected values of $g^{(2)}(\tau)$ calculated based on the static and commercial particle size information are consistent with the experimental data. With the assistance of simulated data, $R_{h,app}$ is discussed. The results show that $R_{h,app}$ is different from the mean hydrodynamic radius and is a composite size determined by the optical, hydrodynamic characteristics and size distribution of particles and scattering vector. The results also reveal that the theoretical value of ρ is determined by not only the structure of particles, but also the relationship between R_s and $R_{h,app}$ even for mono-disperse model.

2 THEORY

For simplicity, poly-disperse homogeneous spherical particles are considered and the RGD approximation is assumed to be valid. The average scattered light intensity of a dilute non-interacting poly-disperse system in unit volume can be obtained for vertically polarized light

$$\frac{I_s}{I_{inc}} = \frac{4\pi^2 \sin^2 \theta_1 n_s^2 \left(\frac{dn}{dc}\right)_{c=0}^2 c 4\pi\rho \int_0^\infty R_s^6 P(q, R_s) G(R_s) dR_s}{\lambda^4 r^2 3 \int_0^\infty R_s^3 G(R_s) dR_s}, \quad (1)$$

where θ_1 is the angle between the polarization of the incident electric field and the propagation direction of the scattered field, c is the mass concentration of particles, r is the distance between the scattering particle and the point of the intensity measurement, ρ is the density of the particles, I_{inc} is the incident light intensity, I_s is the intensity of the scattered light that reaches the detector, R_s is the static radius of a particle, $q = \frac{4\pi}{\lambda} n_s \sin \frac{\theta}{2}$ is the scattering vector, λ is the wavelength of the incident light in vacuo, n_s is the solvent refractive index, θ is the scattering angle, $P(q, R_s)$ is the form factor of homogeneous spherical particles

$$P(q, R_s) = \frac{9}{q^6 R_s^6} (\sin(qR_s) - qR_s \cos(qR_s))^2 \quad (2)$$

and $G(R_s)$ is the number distribution of particle sizes. In this work, the number distribution is chosen as a Gaussian distribution

$$G(R_s; \langle R_s \rangle, \sigma) = \frac{1}{\sigma\sqrt{2\pi}} \exp\left(-\frac{1}{2} \left(\frac{R_s - \langle R_s \rangle}{\sigma}\right)^2\right), \quad (3)$$

where $\langle R_s \rangle$ is the mean static radius and σ is the standard deviation. The number average molar mass is defined as

$$\langle M \rangle = \frac{4\pi\rho}{3} N_A \int_0^\infty R_s^3 G(R_s) dR_s, \quad (4)$$

where N_A represents Avogadro's number.

Comparing with the Zimm plot analysis, the mean square radius of gyration $\langle R_g^2 \rangle_{Zimm}$ for a poly-disperse system is

$$\langle R_g^2 \rangle_{Zimm} = \frac{3 \int_0^\infty R_s^8 G(R_s) dR_s}{5 \int_0^\infty R_s^6 G(R_s) dR_s}. \quad (5)$$

If the reflected light is considered, the average scattered light intensity in unit volume is written as

$$\frac{I_s}{I_{inc}} = a \frac{4\pi\rho \int_0^\infty R_s^6 P(q, R_s) G(R_s) dR_s + b \int_0^\infty R_s^6 P(q', R_s) G(R_s) dR_s}{\int_0^\infty R_s^3 G(R_s) dR_s} \quad (6)$$

where

$$a = \frac{4\pi^2 \sin^2 \theta_1 n_s^2 \left(\frac{dn}{dc}\right)_{c=0}^2 c}{\lambda^4 r^2} \quad (7)$$

and

$$q' = \frac{4\pi}{\lambda} n_s \sin \frac{\pi - \theta}{2} \quad (8)$$

is the scattering vector of the reflected light. b is a constant determined by the shape of sample cell, the refractive indices of the solvent and the sample cell and the geometry of instruments.

For dilute poly-disperse homogeneous spherical particles, the normalized time auto-correlation function of the electric field of the scattered light $g^{(1)}(\tau)$ can be obtained

$$g^{(1)}(\tau) = \frac{\int R_s^6 P(q, R_s) G(R_s) \exp(-q^2 D \tau) dR_s}{\int R_s^6 P(q, R_s) G(R_s) dR_s}, \quad (9)$$

where D is the diffusion coefficient.

From the Einstein-Stokes relation

$$D = \frac{k_B T}{6\pi\eta_0 R_h}, \quad (10)$$

where η_0 , k_B and T are the viscosity of the solvent, Boltzmann's constant and absolute temperature respectively, the hydrodynamic radius R_h can be obtained. For simplicity, the relationship between the static and hydrodynamic radii is assumed to be

$$R_h = k R_s, \quad (11)$$

where k is a constant. From the Siegert relation between $g^{(2)}(\tau)$ and $g^{(1)}(\tau)$ [14]

$$g^{(2)}(\tau) = 1 + \beta \left(g^{(1)}\right)^2, \quad (12)$$

the function between SLS and DLS is built and the values of $g^{(2)}(\tau)$ can be expected based on the particle size information obtained using the SLS technique and the values of $R_{h,app}$ also can be calculated.

3 EXPERIMENT

The SLS and DLS data were measured using the instrument built by ALV-Laser Vertriebsgesellschaft m.b.H (Langen, Germany). It utilizes an ALV-5000 Multiple Tau Digital Correlator and a JDS Uniphase 1145P He-Ne laser to provide a 23 mW vertically polarized laser at wavelength of 632.8 nm.

In this work, two kinds of samples were used. One is PNIPAM submicron spheres. *N*-isopropylacrylamide (NIPAM, monomer) from Acros Organics was recrystallized from hexane/acetone solution. Potassium persulfate (KPS, initiator) and *N,N'*-methylenebisacrylamide (BIS, cross-linker) from Aldrich were used as received. Fresh de-ionized water from a Milli-Q Plus water purification system (Millipore, Bedford, with a 0.2 μm filter) was used throughout the experiments. The synthesis of gel particles was described elsewhere [15,16] and the recipes of the batches used in this work are listed in Table 1. The four samples were named according to the molar ratios n_B/n_N of *N,N'*-methylenebisacrylamide over *N*-isopropylacrylamide.

Sample	T ($^{\circ}$ C)	t (hrs)	$W_N + W_B$ (g)	KPS (mg)	n_B/n_N
PNIPAM-0	70 ± 1	4.0	1.00	40	0
PNIPAM-1	70 ± 1	4.0	1.00	40	1.0%
PNIPAM-2	70 ± 1	4.0	1.00	40	2.0%
PNIPAM-5	70 ± 1	4.0	1.00	40	5.0%

Table 1: Synthesis conditions for PNIPAM particles.

The four PNIPAM samples were centrifuged at 14,500 RPM followed by decantation of the supernatants and re-dispersion in fresh de-ionized water and process was repeated four times to remove free ions and any possible linear chains. Then the samples were diluted for light scattering to weight factors of 5.9×10^{-5} , 8.56×10^{-6} , 9.99×10^{-6} and 8.38×10^{-6} for PNIPAM-0, PNIPAM-1, PNIPAM-2 and PNIPAM-5 respectively. 0.45 μm filters (Millipore, Bedford) were used to clarify the samples PNIPAM-1, PNIPAM-2 and PNIPAM-5 before light scattering measurements. The other kind of samples is two standard polystyrene latex samples from Interfacial Dynamics Corporation (Portland, Oregon). One polystyrene sample is the sulfate polystyrene latex with a normalized mean radius of 33.5 nm (Latex-1) and the other is the surfactant-free sulfate polystyrene latex of 55 nm (Latex-2), as shown in Table 2. Latex-1 and Latex-2 were diluted for light scattering to weight factors of 1.02×10^{-5} and 1.58×10^{-5} respectively.

4 DATA ANALYSIS

In this section, the particle size information included in SLS and DLS and the relationship between SLS and DLS are investigated

4.1 Standard polystyrene latex samples

The particle size information was provided by the supplier as obtained using Transmission Electron Microscopy (TEM) technique. Because of the small particle sizes and the large difference between the refractive indices of the polystyrene latex (1.591 at wavelength 590 nm and 20 °C) and the water (1.332), i.e., the “phase shift” $\frac{4\pi}{\lambda}R|m-1|$ [4, 17] are 0.13 and 0.21 for Latex-1 and Latex-2 respectively, which do not exactly satisfy the rough criterion for validity of the RGD approximation [4], the mono-disperse model $G(R_s) = \delta(R_s - \langle R_s \rangle)$ was used to measure the approximate values of $\langle R_s \rangle$ for the two polystyrene latex samples. The values of the mean radii and standard deviations of the two samples shown in Table 2 were input into Eq. 1 to get I_s/I_{inc} respectively. In order to compare with the experimental data, the calculated value was set to be equal to that of the experimental data at $q = 0.0189 \text{ nm}^{-1}$ for Latex-1. The results are shown in Fig. 1a. In order to compare the expected root mean-square radii of gyration $\langle R_g^2 \rangle_{cal}^{1/2}$ with experimental values $\langle R_g^2 \rangle_{Zimm}^{1/2}$, the values of the mean radii and standard deviations were input into Eq. 5 to calculate $\langle R_g^2 \rangle_{cal}^{1/2}$ respectively. Meanwhile $\langle R_g^2 \rangle_{Zimm}^{1/2}$ was measured using the Zimm plot. Figure 1b shows the fit results of Latex-1: $Kc/R_{vv} = 1.29 \times 10^{-8} + 3.11 \times 10^{-6}q^2$. The DLS data of the two polystyrene latex samples were measured under the same conditions as the SLS data respectively and $R_{h,app}$ was obtained using the first cumulant method. For the two polystyrene latex samples, the values of $R_{h,app}$ at a scattering vector of 0.00905 nm^{-1} were chosen as the results measured using the DLS technique since the values of $R_{h,app}$ almost do not depend on the scattering vector. All results are listed in Table 2. The results show that the difference between the static and apparent hydrodynamic radii is large, the value measured using the SLS technique is consistent with that measured using TEM and the expected value $\langle R_g^2 \rangle_{cal}^{1/2}$ calculated using the commercial size information is consistent with that measured using the Zimm plot analysis.

$\langle R \rangle_{comm}$ (nm)	σ_{comm} (nm)	$\langle R_g^2 \rangle_{Zimm}^{1/2}$ (nm)	$\langle R_g^2 \rangle_{cal}^{1/2}$ (nm)	$\langle R_s \rangle$ (nm)	$R_{h,app}$ (nm)
33.5(Latex-1)	2.5	26.7	26.9	33.3±0.2	37.27±0.09
55(Latex-2)	2.5	46.8	43.2	56.77±0.04	64.5±0.6

Table 2: The commercial size information, values of $\langle R_g^2 \rangle_{Zimm}^{1/2}$, $\langle R_g^2 \rangle_{cal}^{1/2}$, $\langle R_s \rangle$ and $R_{h,app}$ at a scattering vector of 0.00905 nm^{-1} .

If the constant k in Eq. 11 for Latex-1 is assumed to be 1.1 and the size information provided by the supplier is assumed to be consistent with that measured using the SLS technique, all the experimental data and expected values of $g^{(2)}(\tau)$ at a temperature of 298.45 K and the scattering angles 30° , 60° , 90° , 120° and 150° are shown in Fig. 2. The expected values of $g^{(2)}(\tau)$ are consistent with the experimental data.

If the expected values of $g^{(2)}(\tau)$ were calculated using Bargeron's equation [2], all the experimental data and expected values of $g^{(2)}(\tau)$ for Latex-1 at a temperature of 298.45 K and the scattering angles 30° , 60° , 90° , 120° and 150° are shown in Fig. 3. The expected values of $g^{(2)}(\tau)$ have large differences with the experimental data.

5 PNIPAM samples

When Eq. 1 was used to fit the data of PNIPAM-1 measured at a temperature of 302.33 K, it was found that the results of $\langle R_s \rangle$ and σ depend on the scattering vector range being fit, as shown in Table 3. If a small scattering vector range is chosen, the parameters are not well-determined. As the scattering vector range is increased, the uncertainties in the parameters decrease and $\langle R_s \rangle$ and σ stabilize. If the fit range continues to increase, the values of $\langle R_s \rangle$ and σ begin to change and χ^2 grows. This is due to the deviation between the experimental and theoretical scattered light intensity in the vicinity of the scattered intensity minimum around $q = 0.0177 \text{ nm}^{-1}$, where most of the scattered light is cancelled due to the light interference. Many characteristics of particles could influence the scattered light intensity in this region. For example, the number distribution of particle sizes deviates from a Gaussian distribution, the particle shapes deviate from a perfect sphere and the density of particles deviates from homogeneity, etc. In order to avoid the effects of light interference, the stable fit results $\langle R_s \rangle = 254.3 \pm 0.1 \text{ nm}$ and $\sigma = 21.5 \pm 0.3 \text{ nm}$ obtained in the scattering vector range from 0.00345 to 0.01517 nm^{-1} are chosen as the size information measured using the SLS technique. In order to examine the influences of the fit ranges, fitting is also performed in an inverse way where the largest value of q in the fit range is fixed at 0.01517 nm^{-1} while the smallest value of q is varied. The fit results are also listed in Table 3. The results show that $\langle R_s \rangle$ and σ stabilize when the fit range is large enough. Figure 4 shows the stable fit results and the residuals $(y_i - y_{fit})/\sigma_i$ in the scattering vector range from 0.00345 to 0.01517 nm^{-1} , where y_i , y_{fit} and σ_i are the data, the fit value and the uncertainty in the data at a given delay time τ_i , respectively.

When the reflected light was considered, Eq. 6 was used to fit all data in the full scattering vector range (0.00345 to 0.0255 nm^{-1}) for the various factors of reflected light b . The fit results are listed in Table 4. The results show that the values of χ^2 are much larger. The mean static radius $\langle R_s \rangle$ is consistent with that measured using Eq. 1 in the scattering vector range from 0.00345 to 0.01517 nm^{-1} and the standard deviation changes to smaller.

As discussed above, light interference in the vicinity of the scattered intensity minimum would influence the fit results. In order to eliminate the effects of light interference, the experimental data in the vicinity of the scattered intensity minimum were neglected. Eq. 6 was thus used to fit the experimental data in the full scattering vector range again. The fit values are listed in Table 5. The mean static radius and standard deviation are consistent with the stable fit results obtained using Eq. 1 in the scattering vector range from 0.00345 to

q (10^{-3} nm^{-1})	$\langle R_s \rangle$ (nm)	σ (nm)	χ^2
3.45 to 9.05	260.09 ± 9.81	12.66 ± 19.81	1.64
3.45 to 11.18	260.30 ± 1.49	12.30 ± 3.37	1.65
3.45 to 13.23	253.45 ± 0.69	22.80 ± 0.94	2.26
3.45 to 14.21	254.10 ± 0.15	21.94 ± 0.36	2.03
3.45 to 15.17	254.34 ± 0.12	21.47 ± 0.33	2.15
3.45 to 17.00	255.40 ± 0.10	17.32 ± 0.22	11.02
5.50 to 15.17	254.24 ± 0.15	21.95 ± 0.47	2.32
7.95 to 15.17	254.32 ± 0.16	21.56 ± 0.57	2.38
10.12 to 15.17	254.65 ± 0.10	17.81 ± 0.63	0.79
12.21 to 15.17	254.84 ± 0.16	19.33 ± 0.87	0.42

Table 3: The fit results obtained using Eq. 1 for PNIPAM-1 at different scattering vector ranges and a temperature of 302.33 K.

b	$\langle R_s \rangle$ (nm)	σ (nm)	χ^2
0.01	254.0 ± 0.3	14.4 ± 0.5	194.60
0.011	254.0 ± 0.3	14.6 ± 0.5	168.20
0.012	254.0 ± 0.3	14.7 ± 0.5	149.99
0.013	254.0 ± 0.2	14.8 ± 0.4	139.82
0.014	254.1 ± 0.2	15.0 ± 0.4	137.52
0.015	254.1 ± 0.2	15.1 ± 0.4	142.96
0.016	254.09 ± 0.07	15.2 ± 0.5	155.97
0.017	254.1 ± 0.3	15.4 ± 0.5	176.40
0.018	254.1 ± 0.3	15.5 ± 0.5	204.08

Table 4: The fit results for PNIPAM-1 obtained from Eq. 6 using the various values of b .

b	$\langle R_s \rangle$ (nm)	σ (nm)	χ^2
0.013	251.3±0.6	22.17±0.05	79.80
0.014	251.1±0.6	23.3±0.9	58.29
0.015	250.9±0.6	24.4±0.8	44.50
0.016	250.7±0.5	25.4±0.7	37.02
0.017	250.5±0.6	26.4±0.7	36.01
0.018	250.3±0.6	27.24±0.8	41.59

Table 5: The fit results for PNIPAM-1 obtained using Eq. 6 and neglecting experimental data near the intensity minimum.

	$\langle \Gamma \rangle_{first}$	χ^2	$\langle \Gamma \rangle_{two}$	μ_2	χ^2
1	39.73 ±0.07	0.07	39.9 ±0.1	28.20±15.99	0.04
2	39.49 ±0.07	0.33	40.2 ±0.1	90.10±17.11	0.04
3	39.86 ±0.07	0.11	40.2 ±0.1	39.17±16.19	0.05
4	39.70 ±0.07	0.07	39.9 ±0.1	20.93±15.92	0.06
5	39.34 ±0.07	0.53	40.2 ±0.1	112.75±17.26	0.08

Table 6: The fit results of $g^{(2)}(\tau)$ for PNIPAM-1 at a temperature of 302.33 K and a scattering angle of 30°.

0.01517 nm⁻¹.

If the constant k in Eq. 11 for the PNIPAM-1 is assumed to be 1.21, all the experimental data and expected values of $g^{(2)}(\tau)$ at the scattering angles 30°, 50° and 70° are shown in Fig. 5. The expected values of $g^{(2)}(\tau)$ are consistent with the experimental data.

If the expected values of $g^{(2)}(\tau)$ were calculated using Barger's equation, all the experimental data and expected values of $g^{(2)}(\tau)$ for PNIPAM-1 at the scattering angles 30°, 50° and 70° are shown in Fig. 6. The expected values of $g^{(2)}(\tau)$ have large differences with the experimental data.

Traditionally the particle size information is measured using the DLS technique. The standard method is the cumulants or the inverse Laplace transform. For the five experimental data of $g^{(2)}(\tau)$ measured under the same conditions as the SLS data, their corresponding fit results using the first cumulant and first two cumulants respectively for PNIPAM-1 at a temperature of 302.33 K and a scattering angle of 30° are listed in Table 6.

From the fit results, the values of the mean decay rate $\langle \Gamma \rangle$ show an independence on the measurements, but the results of μ_2 have a strong dependence on them. The values of μ_2 are often negative. It's a contradiction with its definition. In order to avoid the contradiction that the values of μ_2 depend on the DLS measurements, the values of $R_{h,app}$ are obtained directly using the first cumulant. The result of $R_{h,app}$ at a scattering angle 30° is 322.±2. nm. The difference between $R_{h,app}$ and $\langle R_s \rangle$ is large.

For the PNIPAM samples at high temperatures, the situation using Eq. 1 is the same as that of PNIPAM-1 at a temperature of 302.33 K. The values of $\langle R_s \rangle$ and σ depend on the scattering vector range being fit. If a small scattering vector range is chosen, the parameters are not well-determined. As the scattering vector range is increased, the uncertainties in the parameters decrease and $\langle R_s \rangle$ and σ stabilize. The stable fit results $\langle R_s \rangle = 139.3 \pm 0.3$ nm and $\sigma = 12.4 \pm 0.6$ nm obtained in the scattering vector range from 0.00345 to 0.02555 nm⁻¹ for PNIPAM-5 at a temperature of 312.66 K are chosen as the size information measured using the SLS technique. Figure 7 shows the stable fit results and the residuals.

If the constant k in Eq. 11 for PNIPAM-5 is assumed to be 1.1, all the experimental data and expected values of $g^{(2)}(\tau)$ at the scattering angles 30°, 50°, 70° and 100° are shown in Fig. 8. The expected values of $g^{(2)}(\tau)$ are consistent with the experimental data. The value of $R_{h,app}$ at a scattering angle 30° is 158.9±0.7 nm. The difference between $R_{h,app}$ and $\langle R_s \rangle$ also is large.

6 RESULTS AND DISCUSSION

Same conclusions are also obtained for all other samples investigated. The fit results of $\langle R_s \rangle$ and σ depend on the scattering vector range being fit. If a small scattering vector range is chosen, the parameters are not well-determined. As the scattering vector range is increased, the uncertainties in the parameters decrease and $\langle R_s \rangle$ and σ stabilize.

For the PNIPAM samples, the main reason for the difference between experimental and theoretical scattered intensity in the vicinity of the scattered intensity minimum seems to be that the number distribution of particle sizes deviates from a Gaussian distribution. With the mean static radius and standard deviation obtained using Eq. 1 in the q range between 0.00345 and 0.01517 nm⁻¹ from the SLS data of PNIPAM-1 measured at a temperature of 302.33 K, three different ways of calculation were performed to see which can give the best expectation of the experimental data. In Fig. 9, the expected values of the scattered intensity related to incident intensity were first calculated using Eq. 1 in the full particle size distribution range between 1 and 800 nm. The calculated curve (solid line) matches the experimental data points only when q is smaller than 0.016 nm⁻¹. Then, a truncated Gaussian distribution was used and the calculation was performed between the $\langle R_s \rangle - 1.3\sigma$ and $\langle R_s \rangle + 1.3\sigma$ using Eq. 1. The calculated curve (dash line) matches the experimental data points in a broad q range including the vicinity of the scattered intensity minimum and deviates only at $q \geq 0.021$ nm⁻¹ where the reflected light could be detected. Finally, the integrated range did not change but the reflected light was considered and Eq. 6 was used to calculate the expected results assuming $b = 0.014$. The calculated curve (dot line) matches the experimental data in all q range investigated. The results show that the scattered intensity in the vicinity of the scattered intensity minimum is very sensitive to the particle size distribution and the influences of the reflected light only lie at very large scattering vectors.

	$\langle \Gamma \rangle_{first}$	χ^2	$\langle \Gamma \rangle_{two}$	μ_2	χ^2
1	39.634 ± 0.002	11.98	39.95 ± 0.01	22.0 ± 0.6	7.75
2	39.252 ± 0.004	4.56	39.49 ± 0.02	9.8 ± 0.6	3.83
3	39.173 ± 0.002	5.67	39.71 ± 0.03	20.6 ± 1.2	4.66
4	39.164 ± 0.004	25.40	39.13 ± 0.01	-1.7 ± 0.4	25.44
5	39.297 ± 0.002	15.75	39.40 ± 0.01	4.9 ± 0.5	15.55

Table 7: The fit results of $g^{(2)}(\tau)$ for the simulated data with the standard deviation 26 nm.

The difference between $\langle R_s \rangle$ and $R_{h,app}$ is large, showing evidences that the different particle sizes for a particle system can be obtained using the light scattering technique. From the theoretical analysis of $\langle R_g^2 \rangle_{Zimm}^{1/2}$, the dimensionless parameter $\langle R_g^2 \rangle_{Zimm}^{1/2} / \langle R_s \rangle$ is determined by the structure of particles and particle size distribution. For mono-disperse homogenous spherical particles, the theoretical value of R_g/R_s is 0.775. Due to the effects of the particle size distribution, the value of $\langle R_g^2 \rangle_{Zimm}^{1/2} / \langle R_s \rangle$ is larger than 0.775. In the analysis of ρ , due to the fact that $R_{h,app}$ and $\langle R_s \rangle$ are different quantities, the value of ρ is also determined by the relationship between them. For the two polystyrene latex samples Latex-1 and Latex-2, the values of ρ are 0.716 and 0.726, respectively.

From the analysis of $g^{(2)}(\tau)$, the expected values of $g^{(2)}(\tau)$ calculated using Eqs 9, 11 and 12 based on the static and commercial particle size information are consistent with the experimental data. The results also reveal that different particle size information is included in $g^{(2)}(\tau)$. In order to discuss this question conveniently, the simulated data are used.

The simulated data were produced using the information: the mean static radius $\langle R_s \rangle$, standard deviation σ , temperature T , viscosity of the solvent η_0 , scattering angle θ , wavelength of laser light λ , refractive index of the water n_s and constant k were set to 260 nm, 26 nm, 302.33K, 0.8132 mPa·S, 30°, 632.8 nm, 1.332 and 1.2, respectively. When the data of $(g^{(2)}(\tau) - 1) / \beta$ were obtained, the 1% statistical noises were added and the random errors were set 3%. Five simulated data were produced. The fit results for the five simulated data using the first cumulant and first two cumulants are listed in Table 7.

From the fit results of the simulated data, the situation is the same as the experimental data: the values of the mean decay rate $\langle \Gamma \rangle$ show an independence on the different noises and errors and the results of μ_2 have a strong dependence on them. The values of μ_2 can be negative. As discussed above, a truncated Gaussian distribution can give better expectation for the SLS data of PNIPAM-1 at a temperature of 302.33 K, so the five simulated data were produced again with the truncated Gaussian distribution that the range of integral is 221 to 299 nm. The fit results for this five simulated data using the first cumulant and first two cumulants respectively are shown in Table 8. The values of μ_2 still have a strong dependence on the different noises and errors and are often negative.

	$\langle \Gamma \rangle_{first}$	χ^2	$\langle \Gamma \rangle_{two}$	μ_2	χ^2
1	39.998 ± 0.001	10.96	39.867 ± 0.009	-5.4 ± 0.4	10.36
2	39.914 ± 0.007	20.57	39.90 ± 0.03	-0.95 ± 1.24	20.63
3	40.045 ± 0.002	5.30	40.35 ± 0.02	12.8 ± 0.8	4.61
4	39.963 ± 0.005	3.97	40.07 ± 0.02	4.3 ± 0.6	3.84
5	39.992 ± 0.003	9.00	40.241 ± 0.008	9.4 ± 0.3	5.51

Table 8: The fit results of $g^{(2)}(\tau)$ for the simulated data produced with a truncated distribution.

$\sigma / \langle R_s \rangle$	$R_{h,app}$ (nm)
5%	315.7 ± 0.9
10%	$325. \pm 2.$
15%	339.4 ± 0.9
20%	$356. \pm 1.$

Table 9: Values of $R_{h,app}$ for the simulated data produced using the same mean static radius and different standard deviations.

Comparing the fit results using the first cumulant with the values using the first two cumulants for the experimental and simulated data respectively, the values of the mean decay rate are consistent. In order to avoid the contradiction that the values of μ_2 depend on the DLS measurements, $R_{h,app}$ is measured using the first cumulant. Meanwhile, from the theoretical analysis of cumulants, $R_{h,app}$ is obtained from averaging the term $\exp(-q^2 D\tau)$ in the static particle size distribution $G(R_s)$ with the weight $R_s^6 P(q, R_s)$. In order to explore the effects of the particle size distribution, the simulated data were produced as the simulated data above with the same mean static radius 260 nm and the different standard deviations 13, 39 and 52 nm respectively. The constant k is still chosen 1.2. From this assumption, the mean hydrodynamic radius is 312 nm. The apparent hydrodynamic radii obtained from $g^{(2)}(\tau)$ for different standard deviations are listed in Table 9.

The results reveal that the values of $R_{h,app}$ are influenced obviously by the standard deviation. As shown in Eq. 9, the quantity $\exp(-q^2 D\tau)$ is determined by the hydrodynamic characteristics while $R_s^6 P(q, R_s)$ is determined by the optical features of particles. As a result, $g^{(2)}(\tau)$ is determined by both the optical and hydrodynamic characteristics of particles. When the cumulants method is used, $R_{h,app}$ obtained from $g^{(2)}(\tau)$ is a composite size determined by the optical, hydrodynamic characteristics and size distribution of particles and scattering vector. If the simple size information needs to be obtained from $g^{(2)}(\tau)$, the relationship between the optical and hydrodynamic quantities must be considered. The accurate relationship between the static and hydrodynamic radii can be explored further.

7 CONCLUSION

Eq. 1 provides a method to accurately measure particle size distribution. Given the absolute magnitude of the scattered intensity and some parameters related to the instrument and samples, the average molar mass of large particles can also be measured accurately. Using the light scattering technique, three different particle sizes can be measured. The static radius is measured from the optical characteristics, the hydrodynamic radius is obtained from the hydrodynamic features and the apparent hydrodynamic radius is determined by the optical, hydrodynamic characteristics and size distribution of particles and scattering vector. With a simple assumption that the hydrodynamic radius R_h is in proportion to the static radius R_s , the expected values of $g^{(2)}(\tau)$ calculated based on the static and commercial particle size information are consistent with the experimental data and the apparent hydrodynamic radius obtained using the cumulants method is different from the mean hydrodynamic radius. The theoretical values of dimensionless shape parameter ρ is related to not only the structure of particles, but also the relationship between the static radius and the apparent hydrodynamic radius even for mono-disperse model. $g^{(2)}(\tau)$ at a scattering vector contains the optical and hydrodynamic information of particles. If the accurate relationship between the optical and hydrodynamic quantities can be understood, the static particle size information can also be measured accurately from DLS.

Fig. 1. a). The experimental data and expected values of I_s/I_{inc} and b). The Zimm plot for Latex-1. In a, the circles show the experimental data and the line represents the expected values of I_s/I_{inc} . In b, the circles show the experimental data and the line shows a linear fit to the plot of Kc/R_{vv} as a function of q^2 .

Fig. 2. The experimental data and expected values of $g^{(2)}(\tau)$ for Latex-1. The symbols show the experimental data and the lines show the expected values calculated under the simple assumption $R_h = 1.1R_s$.

Fig. 3. The experimental data and expected values of $g^{(2)}(\tau)$ for Latex-1. The symbols show the experimental data and the lines show the expected values calculated under the simple assumption $R_h = R_s$.

Fig. 4. The experimental data and stable fit results obtained using Eq. 1 for PNIPAM-1 at a temperature of 302.33 K. The circles show the experimental data, the line shows the fit results and the diamonds show the residuals.

Fig. 5. The experimental data and expected values of $g^{(2)}(\tau)$ for PNIPAM-1 at a temperature of 302.33 K. The symbols show the experimental data and the lines show the expected values calculated under the simple assumption $R_h = 1.21R_s$.

Fig. 6. The experimental data and expected values of $g^{(2)}(\tau)$ for PNIPAM-1 at a temperature of 302.33 K. The symbols show the experimental data and the lines show the expected values calculated under the simple assumption $R_h = R_s$.

Fig. 7. The experimental data and stable fit results obtained using Eq. 1 for PNIPAM-5 at a temperature of 312.66 K. The circles show the experimental data, the line shows the fit results and the diamonds show the residuals.

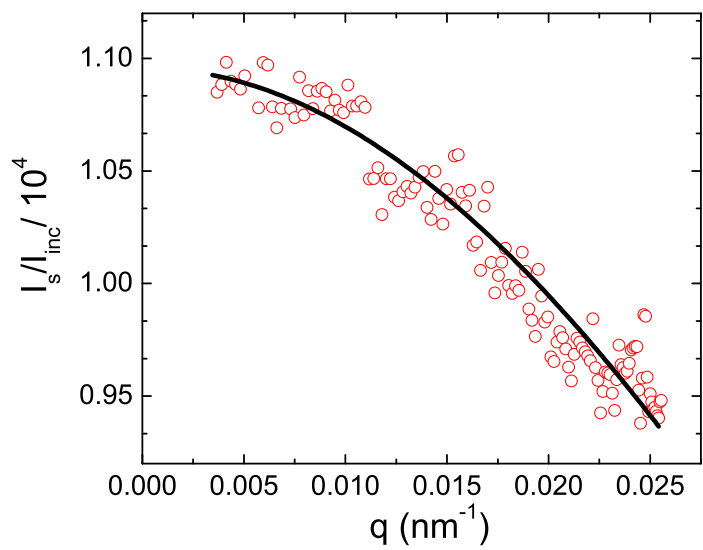
Fig. 8. The experimental data and expected values of $g^{(2)}(\tau)$ for PNIPAM-5 at a temperature of 312.66 K. The symbols show the experimental data and the lines show the expected values calculated under the simple assumption $R_h = 1.1R_s$.

Fig. 9. The experimental data and expected values for PNIPAM-1 at a temperature of 302.33 K. The circles show the experimental data, the solid line shows the expected values calculated using Eq. 1 in the full particle size distribution range, the dash line represents the expected values calculated using Eq. 1 between about the $\langle R_s \rangle - 1.3\sigma$ and $\langle R_s \rangle + 1.3\sigma$ and the dot line shows the expected values calculated using Eq. 6 in the same range as the second with $b: 0.014$.

References

- [1] D. E. Koppel, J. Chem. Phys. **57**, 4814(1972).
- [2] C. B. Barger, J. Chem. Phys. **61**, 2134(1974).
- [3] J. C. Brown, P. N. Pusey and R. Dietz, J. Chem. Phys. **62**, 1136(1975).
- [4] B. J. Berne and R. Pecora, *Dynamic Light Scattering* (Robert E. Krieger Publishing Company, Malabar, Florida, 1990).
- [5] G. Bryant, S. Martin, A. Budi and W. van Meegen, Langmuir **19**, 616(2003).
- [6] W. Burchard, Adv. Polym. Sci. **48**, 1(1983).
- [7] W. Burchard, K. Kajiwara and D. Nergel, J. Polym. Sci. **20**, 157(1982).
- [8] W. Burchard, M. Schmidt and W. H. Stockmayer, Macromolecules **13**, 1265(1980).
- [9] T. Hu and C. Wu, Phys. Rev. Lett. **83**, 4105(1999).
- [10] J. Wu, G. Huang and Z. Hu, Macromolecules **36**, 440(2003).
- [11] P. N. Pusey and W. van Meegen, J. Chem. Phys. **80**, 3513(1984).
- [12] K. B. Strawbridge and F. R. Hallett, Macromolecules **27**, 2283(1994).
- [13] H. Schnablegger and O. Glatter, J. Colloid Interface Sci. **158**, 228(1993).
- [14] P. N. Pusey in *Neutrons, X-rays and Light: Scattering Methods Applied to Soft Condensed Matter*, edited by P. Lindner and Th. Zemb (Elsevier Science B.V., Amsterdam, The Netherlands, 2002).
- [15] J. Gao and B. J. Frisken, Langmuir **19**, 5217(2003).
- [16] J. Gao and B. J. Frisken, Langmuir **19**, 5212(2003).
- [17] H. C. van de Hulst, *Light Scattering by Small Particles* (Dover Publications, Inc. New York, 1981).

a). Fig. 1a



b). Fig. 1b

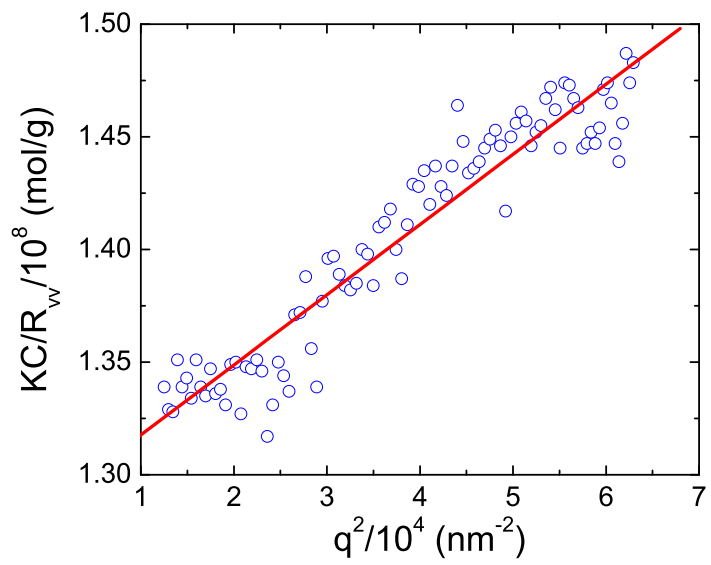


Fig. 2

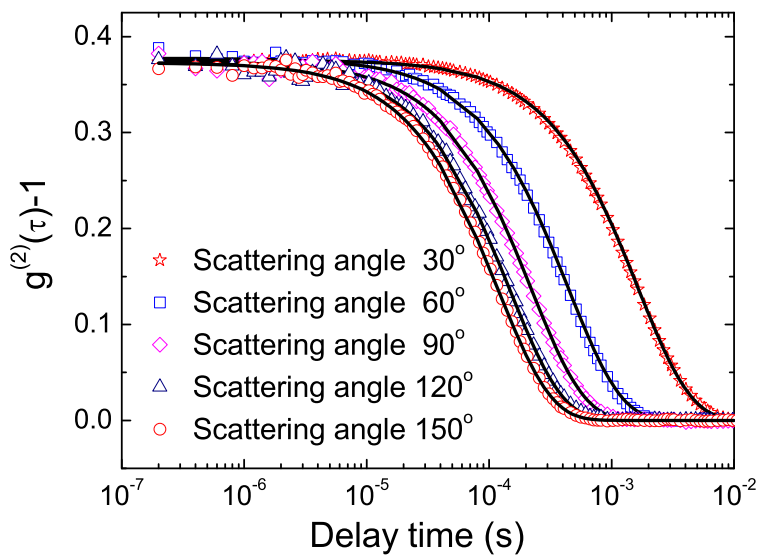


Fig. 3

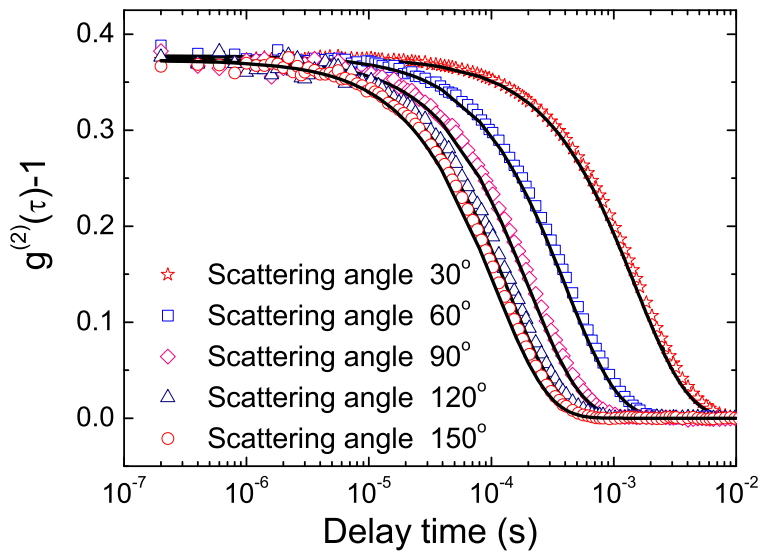


Fig. 4

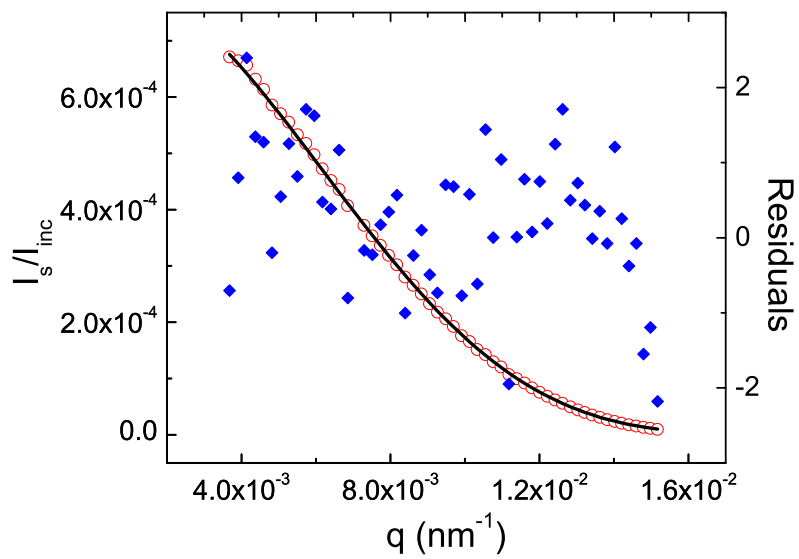


Fig. 5

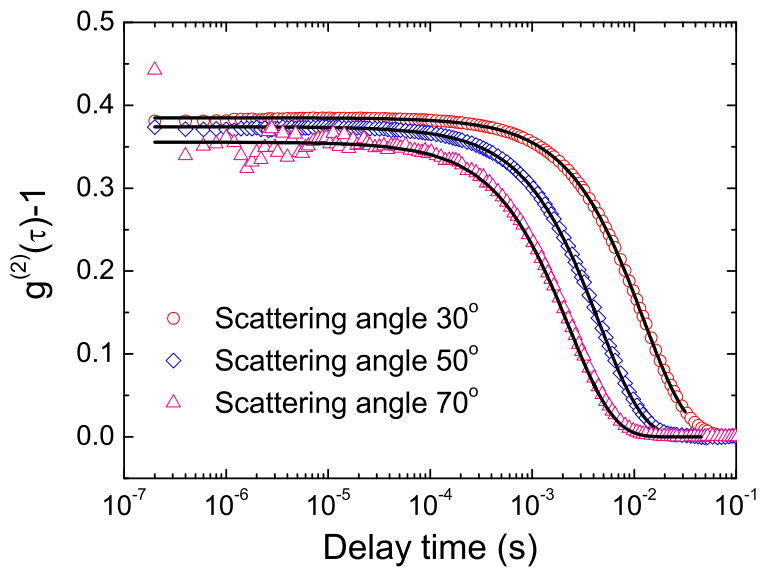


Fig. 6

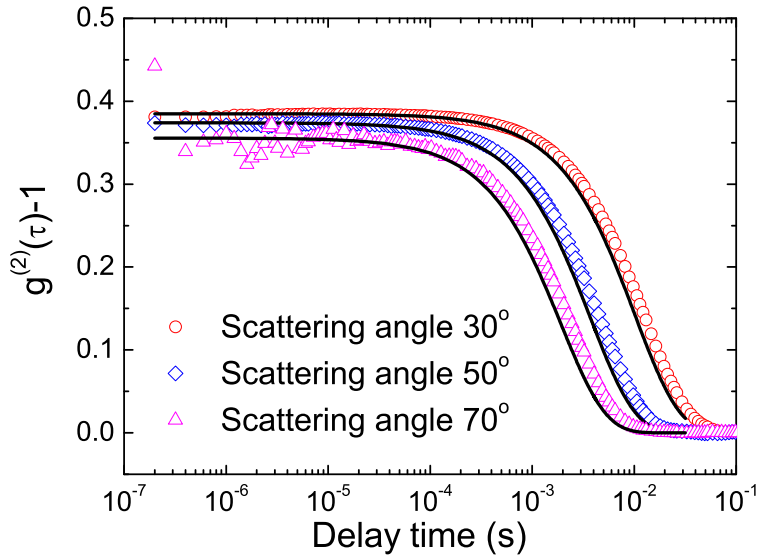


Fig. 7

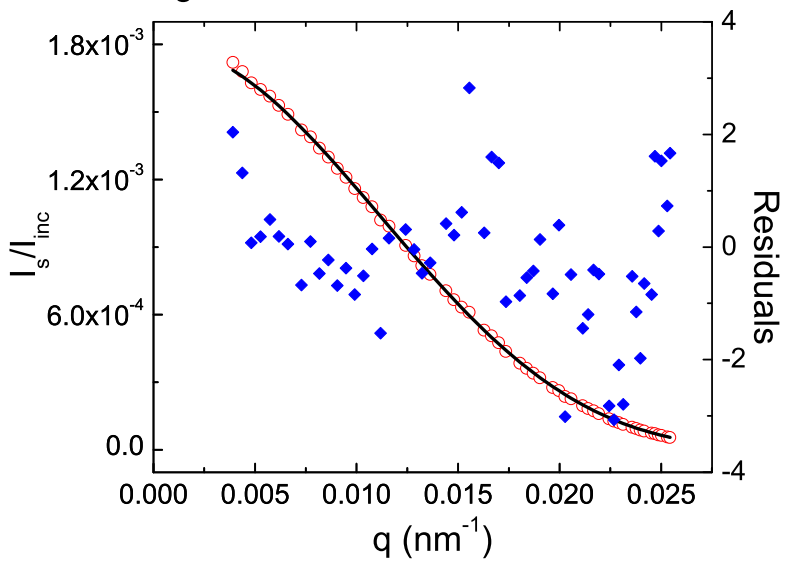


Fig. 8

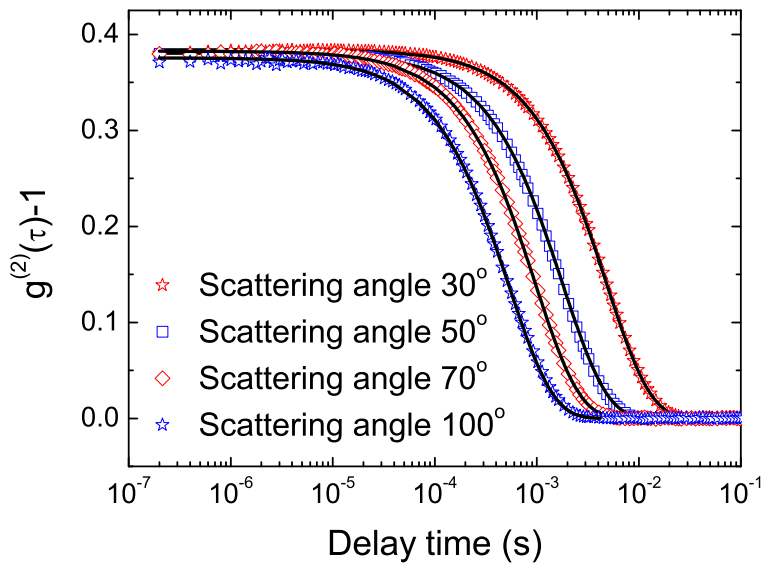


Fig. 9

